GEOSCIENCES

Large-scale and regional climatic influences on surface temperature and precipitation in the South Shetland Islands, northern Antarctic Peninsula

CHRISTIAN TORRES, DENIZ BOZKURT & JORGE ARIGONY-NETO

Abstract: Using data from SCAR observations, ERA5 reanalysis, and regional climate model simulations (RACMO), we examined the influence of large- and regional-scale climate forcing on temperature and precipitation variations in the South Shetland Islands (SSI). Specifically, we focused on understanding how regional climate indices influence the temporal variability of temperature and precipitation on the SSI. Our findings indicate that both large- and regional-scale climate indices significantly impact the interannual and seasonal temperature variability in the SSI. For instance, the Amundsen Sea Low, characterised by low-pressure systems over the Amundsen Sea, and sea ice extent in the northwestern part of the Weddell Sea, exert a strong influence on temperature variability (r from -0.64 to -0.87; p < 0.05). In contrast, precipitation variability in this region is primarily controlled by regional climatic indices. Particularly, anomalies in atmospheric and surface pressure over the Drake Passage region strongly regulate the interannual variability of precipitation in the SSI (r from -0.46 to -0.70; p < 0.05). Large-scale climatic indices demonstrate low but statistically significant correlations, including the Southern Annular Mode and deep convection in the central tropical Pacific. Given the importance of temperature and precipitation in the glacier changes, we recommend assessing the impact of the Drake region on SSI glaciers.

Key words: Temperature, Precipitation, Drake Passage, South Shetland Islands.

INTRODUCTION

Significant changes in key atmospheric variables, such as temperature and precipitation, have been reported over the Antarctic Peninsula (AP) in recent years. Turner et al. (2016) reported a significant warming trend of 0.32 °C/decade over the AP from 1979 to 1997, accompanied by a cooling period (-0.47 °C/decade) between 1999 and 2014 attributed to internal climate variability. More recently, Carrasco et al. (2021) indicated that this warming pause came to an end in the mid-2010s and in another study, the AP is projected to warm for the next two decades (Bozkurt et al. 2021). Carrasco & Cordero (2020) also showed significant increases in precipitation (+16 mm/decade) over the northern AP during the last decades (1970-2020). In addition, Bozkurt et al. (2021) projected positive trends in both temperature and precipitation for the next two decades across the entire AP. Changes in temperature and precipitation are causing significant negative and positive impacts on the cryosphere. For instance, Oliva et al. (2017) indicated positive mass balance in several glaciers located in northern AP from 2006 to 2012, which was apparently associated with a cooling period over the region. Yet, the overall long-term warming trend has caused abrupt

negative changes in the Peninsula's cryosphere (e.g., Sobota et al. 2015, Pudełko et al. 2018, Silva et al. 2020, Shahateet et al. 2021).

Recent studies have analysed the impact of large- and regional-scale climate forcing factors on temperature and precipitation over the AP region. For example, Turner et al. (2020) reported that the interannual and seasonal variability of temperature over the AP is influenced by major climate modes such as the El Niño-Southern Oscillation (ENSO) and Southern Annular Mode (SAM). Similar results were reported for King George Island, located north of the AP by Bello et al. (2022). Carrasco & Cordero (2020) showed that observed monthly precipitation over the northern AP shows statistically non-significant correlations with main climate indices such as ENSO, SAM and Amundsen Sea Low (ASL), indicating that these climate indices have a low influence on precipitation in the region. Gonzalez et al. (2018) indicated that a low-pressure atmospheric circulation system over the Drake Passage strongly influences precipitation over Livingston Island, located north of the AP. Recently, Clem et al. (2022) reported that strong deep convection anomalies in the central tropical Pacific (DC-CPAC) drive high temperatures and surface melt over the Larsen C Ice Shelf located in the eastern part of the AP.

The South Shetland Islands (SSI), located in the northern AP, has been one of the fastest warming regions on Earth since the 1950s and serve as a highly dynamic transitional zone between the subpolar-polar and oceanic-coastal environments (Kerr et al. 2018). The SSI is influenced by different atmospheric forcing from regional (cyclonic and anticyclonic circulations) to global (SAM, ENSO and DC-CPAC) scales (e.g., Marshall & King 1998, Gonzalez et al. 2018, Turner et al. 2016, 2020, Bello et al. 2022, Clem et al. 2022, Marín et al. 2022, Bozkurt et al. 2022). This

region is also influenced by different regional oceanic forcing factors, including sea ice extent-concentration, sea surface temperature, and ocean circulation, encompassing the Bransfield Strait, the Amundsen-Bellingshausen, Drake Passage and Weddell Seas regions (Cook et al. 2016, Kerr et al. 2018). While the role of large-scale climate indices on temperature and precipitation variability has been well studied, the influence of regional-scale climate forcing factors on both temperature and precipitation in this region remains relatively unexplored. In this study, we, therefore, aim to enhance our understanding of how regional climate indices, constructed from anomalies of atmospheric and oceanographic variables in three key regions, impact the interannual and seasonal variability of temperature and precipitation over the SSI. We also examined the temporal variability of the temperature and precipitation in this region over the last four decades (1980-2020). The key contribution of this study is a comprehensive understanding of the role of atmospheric and oceanic forcing factors across three key regions that influence environmental conditions in the SSI, namely the (1) Drake Passage, (2) Amundsen-Bellingshausen, and (3) Weddell Sea regions. By analyzing the impact of these factors on temperature and precipitation variability, we can advance our knowledge of the complex climatic dynamics in this region.

MATERIALS AND METHODS
Study area
The SSI comprise several islands such as King George, Livingston, etc. These islands are located north of the AP and separated by the Bransfield Strait and the Drake Passage (Fig. 1). The climate of these islands is heavily influenced by maritime climatic conditions (Falk et al. 2018) due to their small size and geographical location. Based on
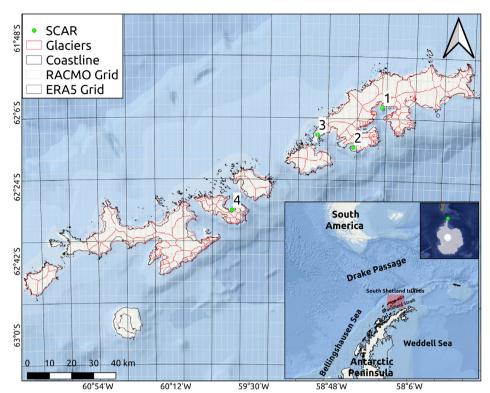
Figure 1. Location map of the South Shetland Islands (SSI), northern Antarctic Peninsula (AP). The green dots indicate the location of the climate stations from east-west (1) Ferraz (Brazil), (2) Carline (Argentina), (3) Bellingshausen (Russia) and (4) Arturo Prat (Chile). The grey grids indicate the spatial resolution of RACMO (~5.5 km horizontal resolution) and the black grids of ERA5 (~31 km horizontal resolution).

the observational data available at the Russian Bellingshausen station, the annual mean temperature is -1.98 ± 0.83 °C, and the annual accumulation of precipitation is 967 ± 115 mm/yr.

Climatological in-situ observations and modelling

Monthly air temperature observations for several climatological stations in Antarctica are available through The Scientific Committee on Antarctic Research (SCAR) READER (https://legacy.bas.ac.uk/met/READER/surface/stationpt.html). For this study, we selected four climatological stations (Bellingshausen, Ferraz, Carlini and Arturo Prat) located on the SSI. Figure 1 shows the station and Table I presentes their names, locations, altitudes, and periods of available data. The selection of these stations was based on the period of available data and their geographic distribution. For instance, Ferraz station is located on the eastern part, while

Arturo Prat station is located on the western part of the SSI. This selection allows us to capture the spatial variability of local temperature on the SSI. These data were extensively used to analyse the temporal variability and trends of air temperature in the region and its relationship with large-scale climate forcings (e.g., Turner et al. 2016, 2020, Oliva et al. 2017, Bello et al. 2022).

Long-term precipitation and consistent observations are very sparse in the Antarctic region. Furthermore, quantifying precipitation in Antarctica involves unique challenges, such as wind and technical difficulties associated with the harsh environment. The strong winds in Antarctica, which can sometimes travel up to 20 m/s, resulting in blowing snow (Van Lipzig et al. 2004), have a profound effect on the accuracy and reliability of precipitation observations. In the SSI, which has a higher concentration of research stations, we found only one climatic station (Bellingshausen Russian Station) that provides freely available monthly precipitation

Table I. List of climatological stations considered in the study.

Station	Operation nation	Available data	Variables	Latitude	Longitude	Elevation (m)
Bellingshausen	Russian Federation	1968-2020	T2, PREC	62.20° S	58.97° W	16
Ferraz	Brazil	1986-2005	T2	62.10° S	58.40° W	20
Carlini	Argentina	1986-2020	T2	62.24° S	58.67° W	4
Arturo Prat	Chile	1966-2020	T2	62.50° S	59.70° W	5

data from 1968 to the present, ensuring the consistency over time. Monthly accumulation precipitation was obtained directly from Bellingshausen Russian Station website (http://www.aari.aq/stations/bell/bell_en.html).

In addition, temperature and precipitation data were obtained from the hourly global ERA5 reanalysis and monthly regional RACMO modelling datasets to compare with observations. ERA5 is a global intermediate spatial resolution atmospheric and oceanic dataset available for the entire globe at ~31 km horizontal resolution (Hersbach et al., 2020). Several studies indicated that the ERA5 dataset provides the most accurate depiction of the recent Antarctic climate (e.g., Gossart et al. 2019, Tetzner et al. 2019, Bozkurt et al. 2020, Hillebrand et al. 2021). RACMO is a regional climate model providing high spatial resolution (5.5 km) of atmospheric and glaciological datasets for the entire AP from 1979 to the present (Van Wessem et al. 2016) (https://www.projects. science.uu.nl/iceclimate/models/racmo-data. php). Van Wessem et al. (2016) found that the RACMO realistically simulates the strong spatial variability, although significant biases remain due to the highly complex topography of the AP.

Some preprocessing steps were applied to the ERA5 and RACMO datasets. First, the ERA5 or RACMO grid closest to each climatic station (see Fig. 1) was selected to obtain the hourly or monthly temperature time series. Next, a bias correction was applied to the temperature data using a constant temperature lapse rate of -1.0°C/100 m for ERA5 and -1.2°C/100 m for RACMO. We use different temperature lapse rates for ERA5 and RACMO because they better reduce the root-mean-square errors (RMSE) at each SCAR station. Finally, in the case of ERA5, hourly temperatures were temporally averaged into daily and monthly time scales. In the case of precipitation, as we only have one climatic station with complete and consistent precipitation data, also of only grid select, we selected all ERA5 or RACMO grids that cover the entire SSI. This allows us to have a better spatial representation of precipitation for the entire SSI. Finally, in the case of ERA5, the hourly data were summed to obtain the monthly cumulative precipitation.

A comparison of the time series between the grids closest to the climate stations and all grids covering the SSI showed no significant differences in both ERA5 and RACMO. This indicates that ERA5 and RACMO do not show large spatial variability in precipitation fields for the entire SSI. Therefore, we used the ERA5 and RACMO precipitation time series obtained from the spatial average of all grids covering the SSI.

Atmospheric and oceanic variables from ERA5 reanalysis

In addition, atmospheric and oceanic variables such as geopotential height at 300 hPa (Z300) and air temperature at 850 hPa (T850), mean sea level pressure (MSLP), sea ice extension (SIE) and sea surface temperature (SST) obtained from the monthly ERA5 reanalysis dataset were used to represent large and regional climatic conditions. The ERA5 hourly and monthly products are freely

available in the Copernicus Climate Data Store (https://cds.climate.copernicus.eu). The main reason for using the ERA5 reanalysis dataset was because it starts from 1940 compared to satellite-derived oceanographic data for sea ice (e.g., US National Snow and Ice Data Center; https://nsidc.org/home) or surface temperature (e.g., Optimum Interpolated OI SST v2; https://www.ncei.noaa.gov/products/optimum-interpolation-sst). Furthermore, the satellite-derived oceanographic data from 1979 to the present and reconstructed from 1979 to 1950 with a sophisticated approach (e.g., Hirahara et al. 2016) were used to force the European Climate System Model that generates the ERA5 reanalysis dataset.

Large and regional climatic indices

The ENSO indices (such as El Niño 3, 3.5 and 4 regions) were obtained from temperature anomalies (https://www.cpc.ncep.noaa.gov/) to represent teleconnection between the Tropic and South Polar regions. Furthermore,

we constructed a custom climatic index that is considered to be large-scale based on outgoing longwave Radiation anomalies in the central Pacific region (hereafter DC-CPAC, see pink in Fig. 2). Recent studies have indicated that deep negative anomalies in the central Pacific region trigger atmospheric rivers landfalling at the AP (Clem et al. 2022). These atmospheric rivers carry large amounts of moisture and heat, which can strongly increase the surface air temperature and surface melting of ice over the AP (Clem et al. 2022). The SAM (https://legacy.bas.ac.uk/met/gjma/sam.htm; monitored using Marshall's (2003) observation-based index) and ASL (https://climatedataguide.ucar.edu/climate-data/amundsen-sea-low-indices) indices were used to represent the large-scale atmospheric circulation of the Antarctic continent (Hosking et al. 2016).

Besides the large-scale indices, we constructed regional-scale climate indices based on the anomalies of Z300, T850, MSLP, SIE, and SST over three key regions: the Drake
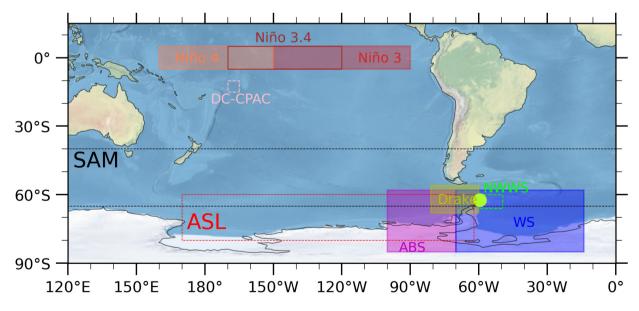

Figure 2. Regions used for the construction of climate indices. Green dot indicates location of the SSI. Amundsen-Bellingshausen (100W-70W; 85S-55S) and Weddell (70W-14W; 85S-55S) Seas regions limits were obtained from Fogt et al. (2022). Drake (81W-60W; 68S-57S) and deep convection anomalies in the central tropical Pacific in the central Pacific (170W-165W; 15S-10S) regions limits were obtained from Clem et al. (2022).

Passage (hereafter Drake; yellow box in Fig. 2), the Amundsen-Bellingshausen Sea (hereafter ABS; magenta box in Fig. 2), and the Weddell Sea (hereafter WS; blue box in Fig. 2), which directly impact the climate in the SSI. All atmospheric and oceanographic variables used to construct our regional indices were obtained from the monthly ERA5 reanalysis dataset. Finally, we also constructed local climate indices based on SIE and SST for a small region located over the Northwestern Weddell Sea (hereafter NWWS) to assess the local effect of SIE and SST conditions on the SSI.

Recent cryosphere-climate studies on the Larsen C Ice Shelf and Patagonian Icefields used similar strategies to construct climatic indices (e.g., Clem et al., 2022, Carrasco-Escaff et al. 2023). We named these time series Z300-Drake, T850-Drake, SST-Drake, SIE-Drake, SST-WS, SIE-WS, SST-ABS and SIE-ABS, respectively.

Statistical analysis

Pearson's correlations analysis were conducted with significance testing based on detrended time series. Interannual time series were computed for the hydrological year in the Southern Hemisphere that starts on 01 April (year n-1) and ends on 31 March (year n). For example, for the year 2000 it starts on 1 April 1999 and ends on 31 March 2000. Standard meteorological season times series for the Southern Hemisphere were used, where DJF represents summer, MAM represents autumn, JJA represents winter, and SON represents spring, where summer begins in December of the previous year.

RESULTS

Interannual and seasonal temperature and precipitation variability

Table II shows the mean, standard deviation (STD), minimum (Min) and maximum (Max) values for annually observed temperature and precipitation (OBS) from the ERA5 reanalysis and RACMO model. Colder and warmer conditions are evident in RACMO (Mean + STD = -2.09 ± 0.78 °C) and ERA5 (Mean + STD = -1.80 ± 0.75 °C), respectively, compared to OBS (Mean + STD = -1.98 ± 0.83 °C). Regarding annual precipitation, ERA5 has the highest value (Mean + STD = 882 ± 80 mm/yr), followed by RACMO (Mean + STD = 872 ± 81 mm/yr) and OBS (Mean + STD = 696 ± 115 mm/yr). In terms of Min values, both OBS (Min = -4.16 °C) and RACMO (Min = -4.02 °C) temperatures are closer compared to ERA5 (Min = -3.59 °C). Although in terms of Max values, OBS (Max = -0.62 °C) and ERA5 (Max = -0.68 °C) temperatures are closer compared to RACMO (Max = -0.50 °C). Precipitation in ERA5 (Min = 733 mm/yr and Max = 1063 mm/yr) and RACMO (Min = 696 mm/yr and Max = 1070 mm/yr) has higher values compared to OBS (Min = 487 mm/yr and Max = 924 mm/yr).

Table II. Annual mean (MEAN), standard deviation (STD), minimum (MIN) and maximum (MAX) values of temperature and precipitation observed and modelled for the time period 1980-2020.

	Temperature (°C)			Precipitation (mm)		
	OBS	**ERA5**	**RACMO**	**OBS**	**ERA5**	**RACMO**
MEAN	-1.98	-1.80	-2.09	696	882	872
STD	0.83	0.75	0.78	115	80	81
MIN	-4.16	-3.59	-4.02	487	733	696
MAX	-0.62	-0.68	-0.50	924	1063	1070

Temperature and precipitation anomalies intercomparison

When comparing the mean annual air temperature anomalies between OBS, ERA5 and RACMO (Fig. 3a) for the average of the four stations, a good performance is observed with high correlation coefficients (r^2 = 0.89 for the ERA5 and RACMO) and low root mean square errors (RMSE = 0.27 °C for the ERA5 and RMSE = 0.30 °C for the RACMO). However, when comparing the cumulative annual precipitation anomalies between OBS, ERA5 and RACMO (Fig. 3b), persistent systematic errors are present with low correlation coefficients (r^2 = 0.06 for ERA5 and r^2 = 0.26 for RACMO) and large root mean square errors (RMSE = 124 mm for ERA5 and RMSE = 100 mm for RACMO). It is important to highlight that from 2006 to 2020 (Fig. 3b), there is a good agreement between the observed and reanalysis-and-modelled precipitation anomalies (ERA5 and RACMO) with higher correlation coefficients (r^2 = 0.73 for ERA5 and r^2 = 0.67 for RACMO) and lower root mean square errors (RMSE = 74 mm for ERA5 and RMSE = 63 mm for RACMO) compared to the full-length time series.

Interannual and seasonal correlation with large- and regional-scale climate indices

As a result of the poor agreement between ERA5, RACMO, and OBS precipitation anomalies, the analysis was conducted independently for observations, ERA5, and RACMO time series.

Interannual temperature variability is influenced by both large- and regional-scale climate indices (Table III). The ENSO 3.4 (r between -0.33 and -0.43) and ENSO 4 (r between -0.40 and -0.49) indices show weak negative but statistically significant correlations with temperature. The ENSO 3 index also shows weak statistically significant for OBS temperature (r = -0.31) and RACMO (r = -0.35), and non-significant for ERA5 (r = -0.24 for ERA5) correlations. Meanwhile, the DC-CPAC index shows weak negative correlations and statistically significant correlations for ERA5 temperature (r = -0.36) and RACMO (r = -0.30). The SAM index (r between 0.45 and 0.48) shows statistically significant positive correlations, and the ASL index (r between -0.64 and -0.71) demonstrates strong negative correlations with annual temperatures over the SSI.
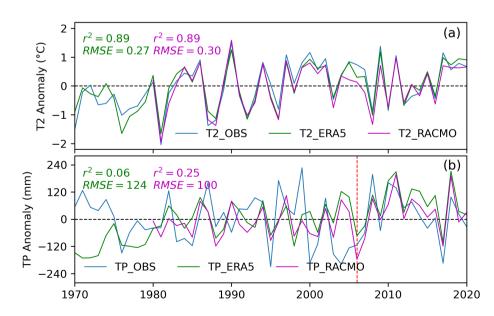

Figure 3. Interannual anomalies for the (a) air temperature and (b) total precipitation over the SSI from 1970 to 2020, as estimated for Observations (blue lines), ERA5 reanalysis (green lines) and RACMO (magenta lines). The vertical red line in (b) indicates the start of 2006.

The interannual variability of precipitation is weakly influenced by the large-scale indices and strongly influenced by two regional climate indices. Large-scale indices such as SAM (r between 0.17 and 0.40) and ASL (r between -0.11 and -0.38) show weak but statistically significant correlations in the ERA5 and RACMO time series. In contrast, all ENSO (3, 3.4 and 4) and DC-CPAC indices show weak but statistically non-significant correlations. Only two regional-scale climate indices associated with atmospheric and surface pressure such as Z300-Drake (r between -0.55 and -0.56) and MSLP-Drake (r between -0.48 and -0.70) over the Drake Passage show strong negative correlations with all OBS, ERA5 and RACMO annual precipitation time series in the SSI.

Since the ASL and MSLP-Drake indices were constructed from the ERA5 MSLP fields and they represented the major controls on the temperature and precipitation, respectively. Therefore, it is reasonable to use these fields to show the main atmospheric circulation patterns that control the variability of temperature and precipitation in the SSI. The spatial correlation analysis map between the annual time series of temperature and precipitation with MSLP fields (Fig. 4) clearly shows that temperature is strongly controlled by MSLP anomalies over the Amundsen Sea, while precipitation is mainly controlled by MSLP anomalies over the Drake region. Furthermore, these results are supported by the time series correlation analysis between the Z300-Drake and MSLP-Drake climate indices shown in Table III and interannual temperature anomalies with ASL index anomalies and precipitation anomalies with MLSP-Drake anomalies shown in Figures 5, 6 and 7.

Table IV presents the correlations between the seasonal temperature OBS, ERA5 and RACMO

Table III. Left three columns show correlation between annual temperature anomalies from Observations, ERA5 and RACMO time series, and large-regional climatic indices. Right three columns show correlation between precipitation anomalies from Observations, ERA5 and RACMO time series, and large-regional climatic indices. Significance is indicated by number asterisk, where * (p < 0.10) and ** (p < 0.05).

	Temperature			Precipitation		
	OBS	**ERA5**	**RACMO**	**OBS**	**ERA5**	**RACMO**
NIÑO 3.4	-0.38**	-0.33**	-0.43**	-0.17	-0.19	-0.19
NIÑO 4	-0.41**	-0.40**	-0.49**	-0.18	-0.23	-0.24
NIÑO 3	-0.31**	-0.24	-0.35**	-0.17	-0.26	-0.25
DC-CPAC	-0.23	-0.36**	-0.30*	-0.06	-0.19	-0.14
SAM	0.46**	0.48**	0.45**	0.17	0.39**	0.40**
ASL	-0.64**	-0.69**	-0.71**	-0.11	-0.37**	-0.38**
SST-ABS	0.27*	0.27*	0.29*	-0.11	-0.12	-0.02
SIE-ABS	-0.47**	-0.43**	-0.49**	-0.06	-0.04	-0.07
SST-WS	0.64**	0.66**	0.67**	-0.02	0.00	0.03
SIE-WS	-0.62**	-0.65**	-0.67**	-0.02	-0.15	-0.14
SST-NWWS	0.77**	0.68**	0.66**	-0.04	-0.01	0.07
SIE-NWWS	-0.88**	-0.84**	-0.81**	0.18	-0.11	-0.17
Z300-Drake	0.16	0.10	0.08	-0.55**	-0.54**	-0.56**
MSLP-Drake	-0.17	-0.27*	-0.27*	-0.48**	-0.69**	-0.70**
T850-Drake	0.68**	0.69**	0.66**	-0.29*	-0.12	-0.03
SST-Drake	0.46**	0.46**	0.47**	-0.20	-0.11	-0.01
SIE-Drake	-0.57**	-0.57**	-0.65**	-0.14	-0.24	-0.30*

with the different climate indices. Regarding the large-scale climate indices, ENSO 3.4 shows higher significant negative correlations during spring (r = -0.39 for the OBS; r = -0.36 for the ERA5; r = -0.46 = for the RACMO) compared to non-significant during autumn (r = -0.14 for the OBS; r = -0.11 for the ERA5; r = -0.16 = for the RACMO). Meanwhile, ENSO 4 shows higher correlations during winter (r = -0.43 for the OBS; r = -0.44 for the ERA5; r = -0.44 = for the RACMO) compared to summer (r = -0.13 for the OBS; r = -0.27 for the ERA5; r = -0.20 = for the RACMO). Similarly to ENSO 3.4, ENSO 3 shows statistically significant correlations during spring (r = -0.37 for the OBS;

r = -0.34 for the ERA5; r = -0.42 = for the RACMO) and non-significant correlations during autumn (r = -0.14 for the OBS; r = -0.09 for the ERA5; r = -0.13 = for the RACMO). SAM and ASL also show significantly stronger signals during winter and spring and weaker signals during summer and autumn, although they remain statistically significant. Clearly, ASL strongly controls the interannual variability of temperature on the SSI, reaching high negative correlations during winter (r = -0.78 for the OBS; r = -0.79 for the ERA5; r = -0.78 = for the RACMO). DC-CPAC shows weak statistically non-significant correlations
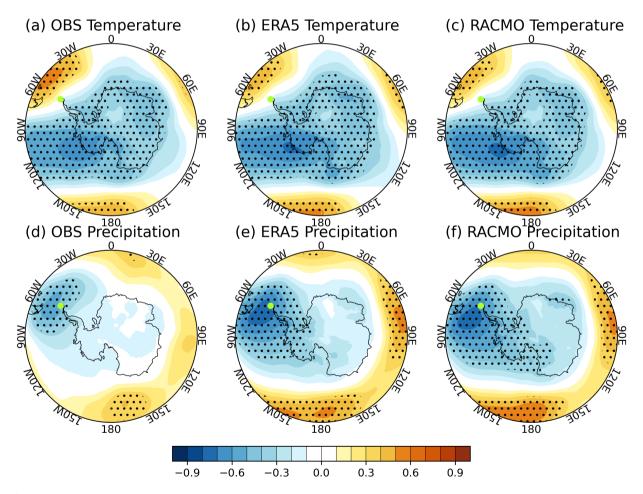

Figure 4. Spatial correlation of the observational data, ERA5 reanalysis and RACMO modelling annual mean temperature (upper plots) and precipitation (bottom plots) time series for 1980–2019 with the spatial annual MSLP from ERA5. The black dots indicate areas where the correlation is significant at p < 0.05. The green dots indicate the location of the SSI.

during spring (r = -0.12 for the OBS; r = -0.25 for the ERA5; r = -0.21 = for the RACMO).

Considering the regional scale climate indices, both SST and SIE over the three key regions considered in this study, such as ABS, WS and Drake (Fig. 2), have stronger signals in temperature during winter and spring compared to summer and autumn. SIE over the Northwestern Weddell Sea even reaches high correlations during winter (r = -0.93 for the OBS; r = -0.93 for the ERA5; r = -0.92 = for the RACMO). Meanwhile, the pressure fields of both the atmosphere and the ocean show weak and statistically non-significant signals in all seasons. In contrast, T850-Drake shows strong positive correlation signals in all temperature seasons and increases during winter and spring.

Table V presents the correlations between the seasonal precipitation from OBS, ERA5 and RACMO with the different climate indices. In context of the large-scale climate indices, ENSO 3.4 indices show significant negative correlations during spring (r = -0.34 for the OBS; r = -0.40 for the ERA5; r = -0.45 = for the RACMO) compared to non-significant during summer, autumn and winter. Similarly, ENSO 3 and 4 show significant negative correlations during spring and non-significant correlations during summer,

autumn and winter. DC-CPAC index shows only a significant correlation during autumn (r = -0.24 for the OBS; r = -0.33 for the ERA5; r = -0.30 = for the RACMO). SAM and ASL show non-significant correlations in all seasons.

Still looking at the regional-scale climate indices, both SST and SIE over the Drake and Weddell Seas show weak significant negative correlations with precipitation during spring (e.g., for SIE-Drake, r = -0.31 for the OBS; r = -0.31 for the ERA5; r = -0.37 = for the RACMO). Z300-Drake climate index shows high significant negative correlations during winter (r = -0.53 for the OBS; r = -0.67 for the ERA5; r = -0.60 = for the RACMO), then during autumn (r = -0.44 for the OBS; r = -0.66 for the ERA5; r = -0.68 = for the RACMO), and finally during spring (r = -0.37 for the OBS; r = -0.44 for the ERA5; r = -0.38 = for the RACMO), while it is non-significant during summer (r = -0.14 for the OBS; r = -0.31 for the ERA5; r = -0.22 = for the RACMO). Similar to the Z300-Drake index, the MSLP-Drake index shows high significant negative correlations during winter (r between -0.43 and -0.76), autumn (r between -0.46 and -0.73) and spring (r between -0.44 and -0.48), and non-significant during summer (r between -0.18 and -0.36). Other climate indices do not show significant correlations.
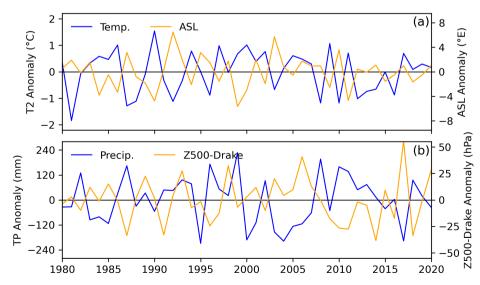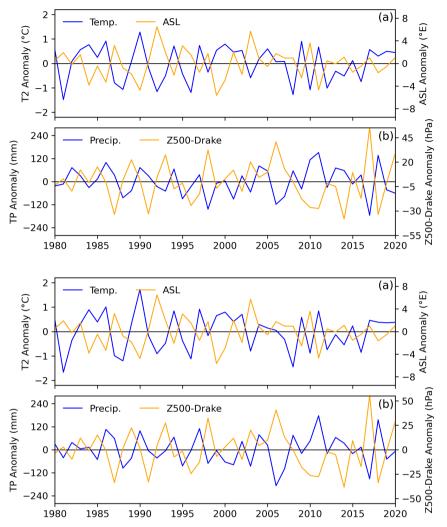

Figure 5. Interannual time series observation of the (a) temperature anomalies (blue) with ASL anomalies index (orange) and (b) precipitation anomalies (blue) with MSLP-Drake anomalies from ERA5 (orange).
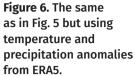
Figure 6. The same as in Fig. 5 but using temperature and precipitation anomalies from ERA5.

Figure 7. The same as in Fig. 5 but using temperature and precipitation anomalies from RACMO.

DISCUSSION

In general, temperature fields from ERA5 and RACMO are in good agreement with observations. However, precipitation fields show low correlations and large RMSE with observations. Several studies indicated that both reanalysis products and regional models (e.g., ERA5 and RACMO) adequately capture temperature but have a poor representation of precipitation, showing strong overestimates over the Antarctic continent (e.g., Gossart et al. 2019, Tetzner et al. 2019, Hillebrand et al. 2021). Interestingly, from 2006 onwards, the annual precipitation anomalies show good agreement with observations (see Fig. 3, $r^2 = 0.73$ for ERA5 and $r^2 = 0.67$ for RACMO). This could be associated with the large uncertainties present in the SSI precipitation observations due to blowing and drifting snow (Tang et al. 2018). It is possible that the strongest correlation can be attributed to the changing atmospheric circulation, as suggested by Bulat Mavlyudov in personal communication, it is particularly noteworthy considering the prevailing cooling conditions during the 2006-2016 period. In addition, it is difficult to assess and draw a robust conclusion that modelled precipitation data do not capture the temporal variability of precipitation well with only one climate station. However, recent intercomparison studies of

Table IV. Correlation between seasonal temperature anomalies (Observation, ERA5 and RACMO time series) and large-regional climatic indices. Significance is indicated by number asterisk, where * (p < 0.10) and ** (p < 0.05).

	Summer			Autumn			Winter			Spring		
	OBS	ERA5	RACMO	OBS	ERA5	RACMO	OBS	ERA5	RACMO	OBS	ERA5	RACMO
NIÑO 3.4	-0.18	-0.36**	-0.30*	-0.14	-0.11	-0.16	-0.29*	-0.29*	-0.32**	-0.39**	-0.36**	-0.46**
NIÑO 4	-0.13	-0.27*	-0.20	-0.26	-0.22	-0.28*	-0.43**	-0.44**	-0.44**	-0.33**	-0.32**	-0.41**
NIÑO 3	-0.20	-0.39**	-0.34**	-0.14	-0.09	-0.13	-0.20	-0.20	-0.23	-0.37**	-0.34**	-0.42**
DC-CPAC	0.05	0.05	-0.01	-0.15	-0.17	-0.18	-0.09	-0.14	-0.18	-0.12	-0.25	-0.21
SAM	0.35**	0.38**	0.48**	0.58**	0.51**	0.61**	0.44**	0.45**	0.39**	0.44**	0.41**	0.47**
ASL	-0.30*	-0.42**	-0.40**	-0.52**	-0.48**	-0.65**	-0.78**	-0.79**	-0.78**	-0.63**	-0.59**	-0.67**
SST-ABS	0.36**	0.35**	0.22	0.32**	0.32**	0.36**	0.42**	0.45**	0.45**	0.31*	0.39**	0.41**
SIE-ABS	-0.40**	-0.38**	-0.33**	-0.31*	-0.23	-0.32**	-0.51**	-0.51**	-0.49**	-0.40**	-0.41**	-0.44**
SST-WS	0.49**	0.61**	0.45**	0.24	0.34**	0.25	0.44**	0.52**	0.56**	0.61**	0.72**	0.73**
SIE-WS	-0.38**	-0.43**	-0.37**	-0.12	-0.21	-0.14	-0.48**	-0.55**	-0.57**	-0.62**	-0.65**	-0.64**
SST-NWWS	0.71**	0.77**	0.64**	0.58**	0.6**	0.45**	0.76**	0.80**	0.80**	0.76**	0.83**	0.80**
SIE-NWWS	-0.70**	-0.63**	-0.58**	-0.67**	-0.69**	-0.53**	-0.93**	-0.93**	-0.92**	-0.81**	-0.85**	-0.81**
Z300-Drake	0.17	0.06	0.08	0.22	0.24	0.21	0.17	0.14	0.13	0.12	0.14	0.04
MSLP-Drake	0.01	-0.15	-0.08	-0.08	-0.04	-0.15	-0.18	-0.22	-0.22	-0.21	-0.19	-0.31*
T850-Drake	0.58**	0.53**	0.46**	0.65**	0.64**	0.68**	0.68**	0.68**	0.69**	0.70**	0.68**	0.69**
SST-Drake	0.55**	0.55**	0.38**	0.36**	0.39**	0.36**	0.55**	0.60**	0.62**	0.36**	0.46**	0.50**
SIE-Drake	-0.29*	-0.27*	-0.23	-0.20	-0.14	-0.24	-0.63**	-0.65**	-0.68**	-0.64**	-0.64**	-0.69**

short-term precipitation derived from remote sensing and modelling indicate that there is a general overestimation in modelled Antarctic precipitation (e.g., Roussel et al. 2020). Therefore, more long-term observations are required to more robustly assess precipitation fields from ERA5 and RACMO or to assess indirectly with glaciological data such as glacier mass balance.

Interannual temperature variability over SSI is primarily controlled by ASL, followed by SAM and ENSO. It is crucial to note that changes in ASL are largely driven by ENSO and other teleconnections (like strong deep convection over the central tropical Pacific) as well as SAM. Therefore, it is essential to recognize that ASL changes are not independent but rather governed by intricate internal dynamics and teleconnections between the tropical and polar (like Southern Hemisphere) regions. For example, Clem et al. (2016) indicated strong correlations between ASL and SAM during summer (r = -0.78), autumn (r = -0.50), winter (r = -0.72) and spring (r = -0.81). They also found that ASL has significant correlations with ENSO during summer (r = 0.35) and winter (r = 0.33). Regional indices such as SIE and SST over the three key regions (i.e. ABS, WS and Drake) also influence the temperature variability. The SIE-NWWS and SST-NWWS indices have higher correlations compared to the remaining large- and regional-scale climate indices. The T850-Drake index also has a high positive correlation with annual temperatures over the SSI. Our results are in agreement with previous studies (e.g., Gonzalez et al. 2018, Turner et al. 2020, Bello et al. 2022). For example, Bello et al. (2022) reported that the interannual temperature variability observed at King George Island exhibits strong, direct and positive correlations with SAM. In addition, Turner et al. (2020) indicated that ASL plays a fundamental role in the AP temperature, altering the meridional component of the wind,

Table V. Correlation between seasonal precipitation anomalies (Observation, ERA5 and RACMO time series) and large-regional climatic indices. Significance is indicated by number asterisk, where * (p < 0.10) and ** (p < 0.05).

	Summer			Autumn			Winter			Spring		
	OBS	ERA5	RACMO	OBS	ERA5	RACMO	OBS	ERA5	RACMO	OBS	ERA5	RACMO
NIÑO 3.4	-0.02	0.07	0.05	0.06	-0.15	-0.15	-0.02	-0.06	-0.12	-0.34**	-0.40**	-0.45**
NIÑO 4	0.08	0.13	0.13	-0.08	-0.16	-0.20	-0.05	-0.12	-0.18	-0.32**	-0.36**	-0.40**
NIÑO 3	-0.05	0.06	0.03	0.11	-0.08	-0.08	0.00	-0.15	-0.20	-0.36**	-0.41**	-0.47**
DC-CPAC	-0.14	-0.16	-0.10	-0.25*	-0.31**	-0.32**	-0.12	0.02	-0.01	0.03	0.10	0.06
SAM	0.04	-0.20	-0.20	-0.04	-0.04	-0.04	-0.18	0.15	0.22	0.33**	0.10	0.12
ASL	-0.15	-0.04	0.10	-0.08	-0.20	-0.21	0.17	-0.14	-0.29*	-0.25	-0.14	-0.22
SST-ABS	-0.16	-0.24	-0.17	0.12	-0.02	0.07	-0.17	0.00	0.14	0.03	0.07	0.11
SIE-ABS	-0.04	0.28*	0.25	0.14	0.03	-0.03	0.26	0.05	-0.08	-0.07	-0.18	-0.19
SST-WS	0.13	0.20	0.17	0.05	-0.03	0.03	0.06	0.16	0.22	0.20	0.32**	0.35**
SIE-WS	-0.12	-0.13	-0.13	-0.23	-0.05	-0.08	-0.06	-0.22	-0.29*	-0.15	-0.37**	-0.37**
SST-NWWS	0.22	0.20	0.19	-0.13	-0.14	-0.09	-0.20	0.15	0.23	-0.03	0.02	0.07
SIE-NWWS	-0.22	-0.08	-0.05	0.08	0.08	0.08	0.32**	-0.08	-0.21	0.10	-0.06	-0.08
Z300-Drake	-0.14	-0.31*	-0.22	-0.44**	-0.66**	-0.68**	-0.53**	-0.67**	-0.60**	-0.37**	-0.44**	-0.38**
MSLP-Drake	-0.18	-0.36**	-0.25	-0.46**	-0.73**	-0.72**	-0.43**	-0.76**	-0.76**	-0.44**	-0.48**	-0.46**
T850-Drake	-0.03	-0.17	-0.11	-0.24	-0.26	-0.28*	-0.29*	-0.15	0.01	0.03	0.00	0.12
SST-Drake	-0.11	-0.19	-0.14	0.03	-0.05	0.05	-0.05	0.19	0.31**	0.09	0.18	0.20
SIE-Drake	-0.06	0.12	0.11	0.12	-0.06	-0.11	0.06	-0.21	-0.32**	-0.31*	-0.31*	-0.37**

which alters the concentration and extent of sea ice over surrounding seas such as Amundsen, Bellingshausen and Weddell and consequently, the heat flux from the ocean to the atmosphere. Furthermore, Gonzalez et al. (2018) indicated that atmospheric low-pressure patterns over Amundsen and Bellingshausen favour the transport of warm and humid air from the Southeast Pacific to the SSI. Similar influences are found to be considerable during the atmospheric blocking patterns over the Drake Passage and AP (Bozkurt et al. 2022).

We find a statistically significant correlation between precipitation anomalies in the SSI and Z300 pressure anomalies in the Drake region (Table III and Figure 4). In general, negative (positive) annual precipitation anomalies are strongly associated with positive (negative) pressure anomalies over the Drake Passage (Table III and Figures 5b, 6b and 7b). This indicates that the Drake region plays a key role in

precipitation over the SSI. In contrast, the large-scale climate indices show low correlations, in some cases significant (such as ASL and SAM) and in others non-significant (such as ENSO and DC-CPAC) in interannual time scale. These results indicate that large-scale climate indices play a less important role in the interannual variability of local precipitation over the SSI. Nonetheless, at regional and decadal scales, these indices have the potential to generate important environmental changes in the AP such as atmospheric circulation, surface temperature and sea ice, leading to changes in decadal precipitation in the region. Our results are in agreement with Carrasco & Cordero (2020), who indicated that monthly precipitation over the northern AP presents low and non-statistical correlations with the main modes of climate variability such as ENSO, SAM and ASL.

There is a consensus among the observed, ERA5 reanalyses and RACMO modelling

precipitation anomalies about the role that the Drake region plays in its interannual variability. Using the time series of observed precipitation anomalies, MSLP anomalies over the Drake play up to 48% (Table III) of its interannual variability. When using the time series of ERA5 and RACMO precipitation anomalies, these MSLP anomalies over Drake can account for up to 69% and 70% (Table III), respectively, over these islands. Similar results were reported by Gonzales et al. (2018), who found that a low-pressure atmospheric circulation pattern over the Drake Passage is associated with large negative and positive precipitation anomalies over Livingston Island, located in the SSI. We note that from 2005 to 2016, the MSLP anomalies over the Drake were consistently negative, leading to positive precipitation anomalies over the SSI during this period (Figs. 5b, 6b, 7b). We hypothesise that anomalously low-pressure in the Drake region indicates a higher density of synoptic-scale cyclones, and precipitation from the trailing cold fronts of these systems is a major contributor to precipitation over the SSI.

While this study does not specifically investigate the teleconnections and mechanisms that potentially cause the Drake low, we can speculate on its origin. It is likely that this pressure feature is influenced by tropical forcing (e.g., Hoskins & Karoly 1981, Karoly 1989, Carrasco-Escaff et al. 2023) and the amplified regional warming and cooling over the AP. For instance, Carrasco-Escaff et al. (2023) argued that the establishment of the Drake low would be highly sensitive to the specific location of SST anomalies in the tropical Pacific, indicating that only certain eastern Pacific SST warming and cooling events could activate an anomalous pressure center near the Drake Passage end to favour annual precipitation and high positive mass balances on Patagonia Icefields. In addition, temperature changes are associated with the

negative (positive) phases of the SAM, increasing (decreasing) the SIE in the northern part of the AP. For example, from 2005 to 2016 (Figs. 5b, 6b and 7b), MSLP over Drake had negative anomalies in most years. This period was indicated as cooling conditions over the AP (e.g., Turner et al. 2016, 2020, Oliva et al. 2017). Furthermore, Turner et al. (2016) indicated that the positive (negative) phase of SAM has warming (cooling) conditions over the northern AP during the last decades (1980 - 2020). Therefore, we suggest further studies must address the understanding of the teleconnections and mechanisms associated with potentially triggering the Drake low.

CONCLUSIONS

The role of different climatic forcing factors on the interannual and seasonal variability of temperature and precipitation over the South Shetland Islands (SSI) was studied from 1980 to 2020 period. Observational data, ERA5 reanalysis and RACMO simulations were used to determine monthly and annual temperature and precipitation anomalies. In addition, different atmospheric (geopotential height, temperature) and oceanic (mean sea level pressure, ice and sea surface temperature) variables from the ERA5 global reanalysis were used to assess their impacts on the seasonal and interannual variability of temperature and precipitation over the SSI. Various large-scale and regional climate indices were constructed based on these atmospheric and oceanic datasets, focusing on three key regions: Weddell (WS), Amundsen-Bellingshausen (ABS), and Drake Passage (Drake) Seas.

We find that the interannual and seasonal variations in air temperature over the SSI are strongly influenced by large- and regional scale climate conditions. Conversely, interannual and seasonal variability of precipitation in this region

is weakly influenced by large-scale climate factors but strongly influenced by regional climate conditions, particularly atmospheric and oceanic pressure anomalies in the Drake region. These pressure anomalies are associated with significant positive and negative precipitation anomalies over the SSI. It is important to note that the indices associated with atmospheric dynamics over Drake (such as Z300-Drake and MSLP-Drake) were statistically significant for precipitation, but did not show such statistically high values for temperature. These results emphasize the crucial role of the Drake region in the temporal variability of precipitation, while its impact on surface temperature over the SSI is relatively less significant. Notable precipitation and temperature changes could directly impact the annual variability of glacier mass balance in the SSI. Hence, it is recommended that future studies consider both large-scale and regional-scale climate modes to gain a better understanding of environmental changes in this region.

Acknowledgments

REFERENCES

BELLO C, SUAREZ W & LAVADO-CASIMIRO W. 2022. Trends and space–time patterns of near-surface temperatures on Maxwell Bay, King George Island, Antarctica. Int J Climatol 42(14): 7426-7442.

BOZKURT D, BROMWICH DH, CARRASCO J, HINES KM, MAUREIRA JC & RONDANELLI R. 2020. Recent near-surface temperature trends in the Antarctic Peninsula from observed, reanalysis and regional climate model data. Adv Atmospher Sci 37: 477-493.

BOZKURT D, BROMWICH DH, CARRASCO J & RONDANELLI R. 2021. Temperature and precipitation projections for the Antarctic Peninsula over the next two decades: contrasting global and regional climate model simulations. Climate Dynamics 56(11-12): 3853-3874.

BOZKURT D, MARÍN JC & BARRETT B S. 2022. Temperature and moisture transport during atmospheric blocking patterns around the Antarctic Peninsula. Weather Climate Extremes 38: 100506.

CARRASCO-ESCAFF T, ROJAS M, GARREAUD RD, BOZKURT D & SCHAEFER M. 2023. Climatic control of the surface mass balance of the Patagonian Icefields. Cryosphere 17: 1127-1149.

CARRASCO JF & CORDERO RR. 2020. Analyzing precipitation changes in the northern tip of the Antarctic Peninsula during the 1970–2019 period. Atmosphere 11(12): 1270.

CARRASCO JF, BOZKURT D & CORDERO RR. 2021. A review of the observed air temperature in the Antarctic Peninsula. Did the warming trend come back after the early 21st hiatus? Polar Science 28: 100653.

COOK AJ, HOLLAND PR, MEREDITH MP, MURRAY T, LUCKMAN A & VAUGHAN DG. 2016. Ocean forcing of glacier retreat in the western Antarctic Peninsula. Science 353(6296): 283-286.

CLEM KR, RENWICK JA, MCGREGOR J & FOGT RL. 2016. The relative influence of ENSO and SAM on Antarctic Peninsula climate. Journal of Geophysical Research: Atmospheres 121(16): 9324-9341.

CLEM KR, BOZKURT D, KENNETT D, KING JC & TURNER J. 2022. Central tropical Pacific convection drives extreme high temperatures and surface melt on the Larsen C Ice Shelf, Antarctic Peninsula. Nature Comm 13(1): 3906.

FALK U, LÓPEZ DA & SILVA-BUSSO A. 2018. Multi-year analysis of distributed glacier mass balance modelling and equilibrium line altitude on King George Island, Antarctic Peninsula. Cryosphere 12(4): 1211-1232.

FOGT RL, SLEINKOFER AM, RAPHAEL MN & HANDCOCK MS. 2022. A regime shift in seasonal total Antarctic sea ice extent

in the twentieth century. Nature Climate Change 12(1): 54-62.

GONZALEZ S, VASALLO F, RECIO-BLITZ C, GUIJARRO JA & RIESCO J. 2018. Atmospheric patterns over the Antarctic Peninsula. J Climate 31(9): 3597-3608.

GOSSART A, HELSEN S, LENAERTS JTM, BROUCKE SV, VAN LIPZIG NPM & SOUVERIJNS N. 2019. An evaluation of surface climatology in state-of-the-art reanalyses over the Antarctic Ice Sheet. J Climate 32(20): 6899-6915.

HERSBACH H ET AL. 2020. The ERA5 global reanalysis. Q J R Meteorol Soc 146(730): 1999-2049.

HIRAHARA S, BALMASEDA MA, DE BOISSESON E & HERSBACH H. 2016. Sea Surface Temperature and Sea Ice Concentration for ERA5, p. 25. ECMWF ERA Report Series 26.

HILLEBRAND FL, BREMER UF, ARIGONY-NETO J, DA ROSA CN, MENDES JR CW, COSTI J, DIAS DE FREITAS MW & SCHARDONG F. 2021. Comparison between atmospheric reanalysis models ERA5 and ERA-Interim at the North Antarctic Peninsula region. Ann Amer Assoc Geograph 111(4): 1147-1159.

HOSKINS BJ & KAROLY DJ. 1981. The steady linear response of a spherical atmosphere to thermal and orographic forcing. J Atmospher Sci 38(6) 1179-1196.

HOSKING JS, ORR A, BRACEGIRDLE TJ & TURNER J. 2016. Future circulation changes off West Antarctica: Sensitivity of the Amundsen Sea Low to projected anthropogenic forcing. Geophys Res Lett 43(1): 367-376.

KAROLY DJ. 1989. Southern hemisphere circulation features associated with El Niño-Southern Oscillation events. J Climate 2(11): 1239-1252.

KERR R, MATA MM, MENDES CRB & SECCHI ER. 2018. Northern Antarctic Peninsula: a marine climate hotspot of rapid changes on ecosystems and ocean dynamics. Deep Sea Res Part II Top Stud Oceanogr 149: 4-9.

MARÍN JC, BOZKURT D & BARRETT BS. 2022. Atmospheric blocking trends and seasonality around the Antarctic Peninsula. J Climate 35(12): 3803-3818.

MARSHALL GJ & KING JC. 1998. Southern Hemisphere circulation anomalies associated with extreme Antarctic Peninsula winter temperatures. Geophys Res Lett 25(13): 2437-2440.

MARSHALL GJ. 2003. Trends in the Southern Annular Mode from observations and reanalyses. J Climate 16(24): 4134-4143.

OLIVA M, NAVARRO F, HRBÁČEK F, HERNANDÉZ A, NÝVLT D, PEREIRA P, RUIZ-FERNÁNDEZ J & TRIGO R. 2017. Recent regional climate cooling on the Antarctic Peninsula and associated impacts on the cryosphere. Sci Total Environ 580: 210-223.

PUDEŁKO R, ANGIEL PJ, POTOCKI M, JĘDREJEK A & KOZAK M. 2018. Fluctuation of glacial retreat rates in the eastern part of Warszawa Icefield, King George Island, Antarctica, 1979–2018. Remote Sensing 10(6): 892.

ROUSSEL ML, LEMONNIER F, GENTHON C & KRINNER G. 2020. Brief communication: Evaluating Antarctic precipitation in ERA5 and CMIP6 against CloudSat observations. Cryosphere 14: 2715–2727.

SILVA AB, ARIGONY-NETO J, BRAUN MH, ESPINOZA JMA, COSTI J & JAÑA R. 2020. Spatial and temporal analysis of changes in the glaciers of the Antarctic Peninsula. Global Planet Change 184: 103079.

SHAHATEET K, SEEHAUS T, NAVARRO F, SOMMER C & BRAUN M. 2021. Geodetic Mass Balance of the South Shetland Islands Ice Caps, Antarctica, from Differencing TanDEM-X DEMs. Remote Sens 13(17): 3408.

SOBOTA I, KEJNA M & ARAŹNY A. 2015. Short-term mass changes and retreat of the Ecology and Sphinx glacier system, King George Island, Antarctic Peninsula. Antarctic Sci 27(5): 500-510.

TANG M S, CHENOLI S N, SAMAH AA & HAI OS. 2018. An assessment of historical Antarctic precipitation and temperature trend using CMIP5 models and reanalysis datasets. Polar Sci 15: 1-12.

TETZNER D, THOMAS E & ALLEN C. 2019. A validation of ERA5 reanalysis data in the Southern Antarctic Peninsula—Ellsworth land region, and its implications for ice core studies. Geosci 9(7): 289.

TURNER J, LU H, WHITE I, KING JC, PHILLIPS T, HOSKING JS, MULVANEY R & DEB P. 2016. Absence of 21st century warming on Antarctic Peninsula consistent with natural variability. Nature 535(7612): 411-415.

TURNER J, MARSHALL GJ, CLEM K, COLWELL S, PHILLIPS T & LU H. 2020. Antarctic temperature variability and change from station data. Int J Climatol 40(6): 2986-3007.

VAN LIPZIG NPM, TURNER J, COLWELL SR & VAN DEN BROEK MR. 2004. The near-surface wind field over the Antarctic continent. Int J Climatol: A Journal of the Royal Meteorological Society 24(15): 1973-1982.

VAN WESSEM JM ET AL. 2016. The modelled surface mass balance of the Antarctic Peninsula at 5.5 km horizontal resolution. Cryosphere 10(1): 271-285.

CHRISTIAN TORRES[1,2]
https://orcid.org/0000-0001-5530-2119

DENIZ BOZKURT[2,3,4]
https://orcid.org/0000-0003-1021-8241

JORGE ARIGONY-NETO[1]
https://orcid.org/0000-0003-4848-2064

[1]Universidade Federal do Rio Grande/FURG, Instituto de Oceanografia, Av. Itália, s/n, Km 8, 96201-900 Rio Grande, RS, Brazil

[2]Universidad de Valparaíso, Departamento de Meteorología, Gran Bretaña 644, 2340000, Playa Ancha, Valparaíso, Chile

[3]Universidad de Chile, Center for Climate and Resilience Research (CR)2, Blanco Encalada 2002, 4th floor, 8330015, Santiago, Chile

[4]Universidad de Concepción, Center for Oceanographic Research COPAS COASTAL, Edmundo Larenas 219, 4070409, Concepción, Chile

Correspondence to: **Christian Torres**
E-mail: christian010194@gmail.com

Author contributions

Christian Torres was responsible for pre-processing data, statistical analysis, and writing of the manuscript. Deniz Bozkurt and Jorge Arigony-Neto performed discussion of the results, and final revision of the manuscript.